Time dependence of fast electron beam divergence in ultraintense laser-plasma interactions

K. U. Akli, M. J. Storm, M. McMahon, S. Jiang, V. Ovchinnikov, D. W. Schumacher, and R. R. Freeman
The Ohio State University, Columbus, Ohio 43210, USA

G. Dyer and T. Ditmire
University of Texas at Austin, Austin, Texas 78712, USA

(Received 29 May 2012; revised manuscript received 25 June 2012; published 14 August 2012)

We report on the measurement and computer simulation of the divergence of fast electrons generated in an ultraintense laser-plasma interaction (LPI) and the subsequent propagation in a nonrefluxing target. We show that, at $I\lambda^2$ of 10^{20} Wcm^{-2} μm^2, the time-integrated electron beam full divergence angle is $(60 \pm 5)^\circ$. However, our time-resolved 2D particle-in-cell simulations show the initial beam divergence to be much smaller ($\leqslant 30^\circ$). Our simulations show the divergence to monotonically increase with time, reaching a final value of $(68 \pm 7)^\circ$ after the passage of the laser pulse, consistent with the experimental time-integrated measurements. By revealing the time-dependent nature of the LPI, we find that a substantial fraction of the laser energy ($\sim$7%) is transported up to 100 μm with a divergence of 32°.

DOI: 10.1103/PhysRevE.86.026404 PACS number(s): 52.38.−r, 52.50.Jm

I. INTRODUCTION

The interaction of an ultraintense laser with solid targets—the so called laser-plasma interaction (LPI)—is of great interest to many applications, including isochoric heating of matter [1–3], proton and heavy ion acceleration [4–6], bright x-ray sources [7], and electron-positron pair production [8]. Advancing and optimizing these applications requires understanding the physics of the generation of the fast electrons by ultraintense lasers and their subsequent transport in solid density matter.

There are many experimental factors that affect the general characteristics of the LPI; electron beam source size, mean energy, energy distribution, and divergence. These include the laser pulse profile, target material, and combinations of the two. Most ultraintense lasers have an inherent amplified spontaneous emission (ASE) pedestal that precedes the main pulse on a nanoseconds scale. This pedestal is often intense enough to preionize the target creating a preformed plasma with which the main pulse interacts. This preformed plasma is known to affect both the laser pulse propagation and the electron beam generation [9]. Although the preformed plasmas can hinder some applications such as fast ignition [10], it is desirable in many others. For example, long scale preformed plasmas generate an extremely energetic tail in the electron energy distribution that can benefit laser wake field acceleration, bright x-ray sources, and electron-positron pair production.

The laser-generated electron beam divergence angle has recently received a lot of attention in laser-plasma interaction experiments. Various techniques have been used to measure this parameter: e.g., K_α fluorescence measurements [11,12], coherent transition radiation (CTR) [13], and Planckian emission imaging [14]. The published full angle values for the beam divergence range from 30° to as much as 100°. One of the reasons for the discrepancy in the reported values is that experiments are carried out with thin targets where the electron trapping and circulation, due to the electrostatic sheath that forms around the target, complicates the data interpretation [15,16].

There is a developing consensus in the high energy density physics community that the ultraintense laser-generated electron beam divergence angle is larger than can be tolerated for some applications such as fast ignition, consistent with the measurements of Green *et al.* (2008). However, this conclusion is based on time-integrated measurements and only applies to the final beam divergence. Here we argue that it is meaningless to talk about a single beam divergence value since the measurements are affected by time-dependent local magnetic fields and target surface electric fields, which also vary in time. In many, if not most applications, the useful figure of merit is not the time-integrated beam divergence angle but rather the spatial spread of the fast electrons as a function of time and the distribution of energy they represent at a given time. For example: How do the electron beam flux and energy transport evolve with time? Do these quantities significantly change before and after the laser pulse is off?

In this paper, we report on electron beam divergence measurements using nonrelaxing targets. We use the particle-in-cell (PIC) code Large Scale Plasma (LSP) to model these massive targets to get insight into the time-dependent behavior of electron beam divergence and energy transport. In what we believe to be a first, the simulations include not only a full LPI with spatial and time resolution sufficient to represent all of the relevant dynamics, but the subsequent transport of the fast electrons, including dynamic ionization, and electron scattering, throughout an extended target.

II. EXPERIMENTAL SETUP AND RESULTS

The experiments were conducted on the Texas Petawatt laser system at the University of Texas at Austin. The laser delivered 50 J of energy at a wavelength of 1.054 μm. The pulse length, measured with a second order autocorrelator, was 250 fs full width at half maximum intensity (FWHM). The laser beam was focused with an f/3 off-axis parabola and the intensity distribution was determined by imaging the focal spot at low power. The peak laser intensity was 1.2×10^{20} Wcm^{-2} with 50% of the energy focused in excess

 ©2012 American Physical Society

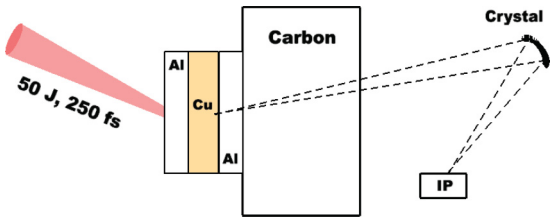

FIG. 1. (Color online) Experimental setup: A 50 J, 250 fs laser pulse incident on Al-Cu-Al-C target. The K_α photons induced by electrons in Cu are collected using a spherically bent Bragg crystal.

of 2.5×10^{19} Wcm^{-2}. The prepulse was not monitored during this experiment. However, the preformed plasma scale length was about 1.5 μm, indirectly determined from the sensitivity of the K_α images to prepulses [16], as discussed in Sec. III. The laser beam irradiated the Al-Cu-Al-C targets at 30° angle of incidence (Fig. 1). The thickness of the Al layer in front of the 25-μm Cu tracer layer was 15, 50, or 100 μm. The Al layer behind Cu was 20 μm thick. To minimize rear and side electron refluxing, a large carbon layer was fixed to the rear side of the target to act as a fast electron absorber. This layer was 1 mm thick and 5×10 mm in the transverse direction.

The K_α photons induced by electrons in Cu were collected using a spherically bent Bragg Quartz crystal [17]. The photons were then detected with BAS-MS 2040 imaging plates and scanned with a Fuji FLA7000 scanner to obtain 2D spatially resolved images of the target. Figure 2(a) shows typical experimental data along with the horizontal lineout. The two-dimensional image in the figure is a time-integrated spatial distribution of K_α emission induced in the Cu layer by laser-generated electrons. The horizontal lineout is averaged over 10 pixels and shows an emission spot of 80 μm full width at half intensity.

The time-integrated electron beam divergence angle is determined from K_α emission radii at various depths. Figure 2(b) is a plot of the K_α radius as a function of the Cu layer depth. Each data point represents the radius averages over a few shots with the error bars reflecting the standard deviation. A linear fit to this set of data is found using a weighted least square fit. The time-integrated electron beam divergence was determined from the slope of the linear fit to be $(60 \pm 5)^\circ$ full cone angle. This divergence angle is consistent with the values of $(58 \pm 7)^\circ$ and $(70 \pm 13)^\circ$ reported by Green *et al.* at laser intensities of 1.5×10^{19} Wcm^{-2} and 4×10^{19} Wcm^{-2}, respectively [12].

III. 2D HYBRID-PIC SIMULATIONS: TIME-DEPENDENCE OF FAST ELECTRON BEAM DIVERGENCE AND FLUX

To reveal the time-dependence of the electron beam transport during and after the laser pulse, we have carried out full-scale 2D implicit PIC simulations using LSP [18]. The 1-μm wavelength laser pulse was modeled as a sine-square function in time with a 250 fs FWHM. The 50 J laser pulse spatial profile was modeled as a Gaussian with 15-μm FWHM. The simulations were carried out in xz Cartesian geometry with the laser propagating in the x direction. After propagating through a 40-μm vacuum region, the laser enters a low density preplasma region with a 1.5-μm scale length. The interaction of the laser with the preplasma takes into account dynamic

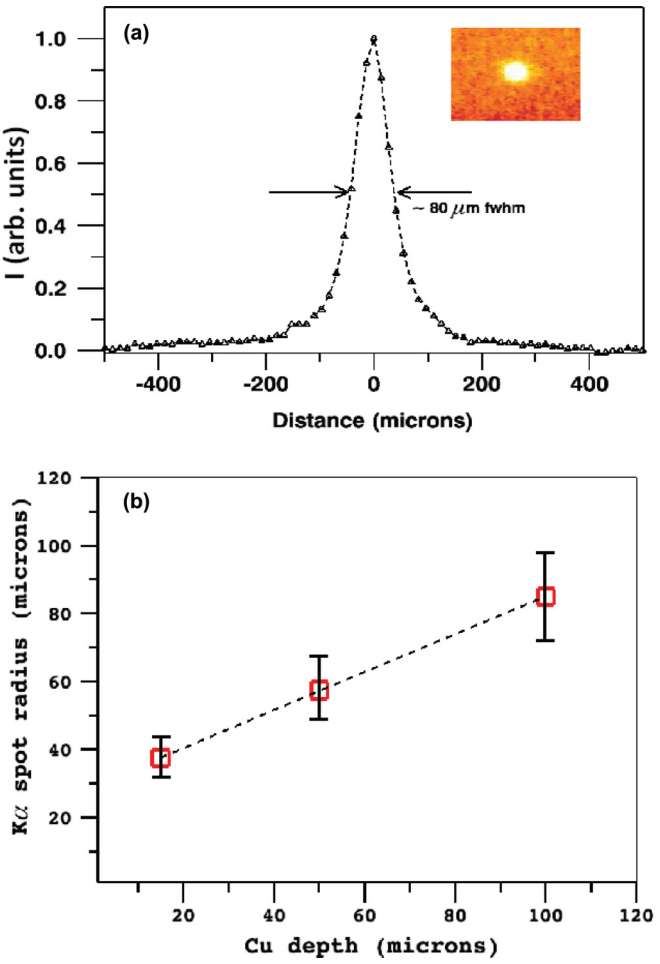

FIG. 2. (Color online) (a) Typical experimental data: A K_α image with Cu tracer at a depth of 15 μm (inset); a horizontal lineout of the image showing an 80-μm spot size full width at half intensity. (b) Experimental K_α radius as a function of Cu depth. Full divergence angle of $(60 \pm 5)^\circ$ is determined by weighted least square fit.

ionization using the Ammosov-Delone-Krainov (ADK) model [19]. Segmented ionization through all ionization states was modeled on every time step. The spatial resolution starts at $\lambda/8 \times \lambda/8$ in the LPI region and linearly increases to $\lambda \times \lambda$ over 50 μm in the x direction, remaining constant thereafter. The region adjacent to the preplasma had an initial solid density, was initially singly ionized, and had a temperature of 5 eV. Electron scattering was treated using the Lee-More-Desjarlias collision model [20]. The carbon layer was modeled as a sink of electrons, as intended in the experiment, using the "conductor" model in LSP.

K_α emission induced by electron impact ionization was modeled by the integrated Tiger series (ITS) [21] code implemented in LSP. Five different depths (0, 15, 50, 75, and 100 μm) were taken as K_α extraction planes. The experimental K_α images were first used to determine the preplasma profile scale length in the vicinity of the critical surface following the technique we recently introduced [16]. Briefly, the scale length was used as a single fitting parameter to match the K_α image profiles at all target depths. As explained in our previous work, images at different depths, and different regions of the same image at a given depth, have varying dependence to changes in

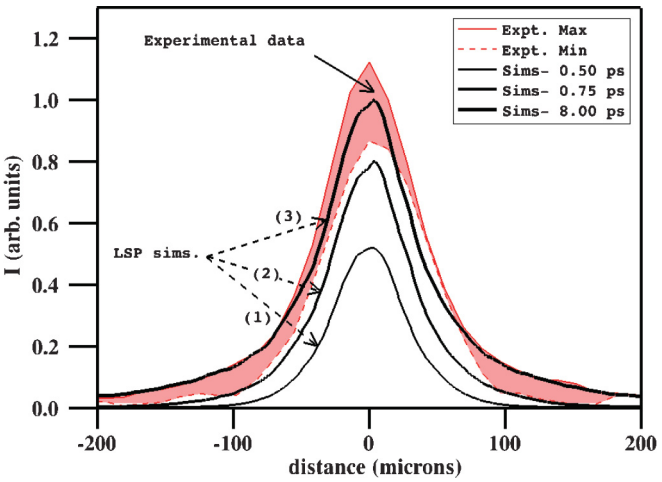

FIG. 3. (Color online) Time evolution of K_α emission at a depth of 15 μm. The red band represents the range of the time-integrated experimental data. Black curves are the K_α profiles obtained from simulations at 0.50, 0.75, and 8.00 ps from bottom to top, respectively.

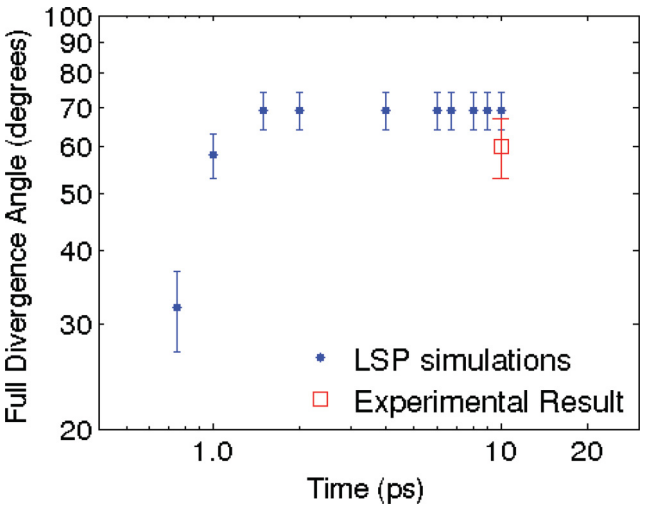

FIG. 5. (Color online) Time-dependent beam divergence from LSP simulations (solid circles). Time-integrated experimental measurement (square).

scale length making this a sensitive technique. For this work, we found a preplasma scale length of (1.5 ± 0.3) μm.

Figure 3 shows the time evolution of the simulated K_α emission at a depth of 15 μm. The black curves labeled (1) and (2) in Fig. 3 are the K_α profiles obtained from simulations at 0.50 and 0.75 ps, respectively. Curve (3), the simulated profile after 8.00 ps, is in good agreement with the time-integrated experimental data range indicated by the red band. The time-dependent behavior of K_α emission at various depths is shown in Fig. 4. It is clear that the spot size increases with time and continues to increase even after the laser pulse is off. The rate at which the spot size increases is greater in the deeper planes as the most energetic electrons arrive there first. Closer to the laser-target interaction region, the growth rate is less as both fast and slow electrons contribute to the emission. Moreover, this rate is also affected by electrons that reflux from the front surface electrostatic sheath and return to the target where they contribute to the K_α emission. The increase in the K_α spot

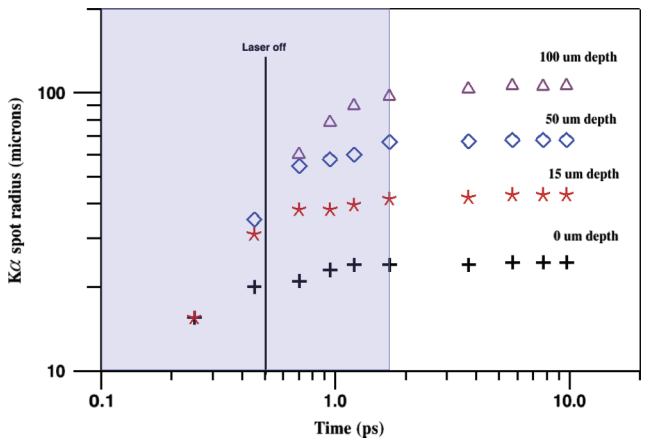

FIG. 4. (Color online) Time evolution of K_α spot size at 0-, 15-, 50-, and 100-μm depths. The shaded area is the region of monotonically increasing K_α spot size. In the nonshaded area, the spot size becomes constant.

radius is followed by a plateau region, which starts at about 1.7 ps and is depth independent. At any given time, the electron beam divergence is determined from the slope of the linear fit to the K_α spot radii at various depths. The time-dependent divergence is plotted in Fig. 5. It is clear that the initial beam divergence is small. This divergence increases monotonically with time and reaches a plateau in less than 2 ps. The final beam divergence is $(68 \pm 7)^\circ$, consistent with the time-integrated experimental measurements.

To determine the time-dependent energy transport at various depths in the target, we use the K_α spot size and the corresponding electrons that induced the emission. At a given depth and given time, we first determine the K_α emission distribution in space. The full width at half maximum of the profile is then taken as a measure of the spot size. With this information and after computing the electron energy distribution that induced the emission, the time-dependent electron beam flux is determined. The relationship between the fluxes at the three emission depths from the experiment and the beam divergence are shown in Table I. As the electron beam evolves with time, the flux decreases. For the 32° beam divergence angle, the fluxes at depths of 50 and 100 μm are 92% and 21% that of 15 μm, respectively. In the calculation, we have included all electrons above 9 keV. The electron energy spectrum throughout the target has two populations: a hot population that can be described with a Boltzmann distribution and a lower-energy population. The hot tail of the distribution has a temperature of 7 MeV consistent with the ponderomotive scaling [22]. The laser-to-electron conversion efficiency in our experiment is determined by our simulations to be ~45%, similar to the value reported by Yasuike *et al.* (2001) at 3×10^{20} Wcm^{-2} laser intensity [23].

Of current interest is the transport of the hot electron population, especially electrons with energy above 1 MeV that can carry energy deep into the target due to their long mean free path. We have looked at the transport of these electrons as they pass through an extraction plane as a function of time. We

TABLE I. Time-dependent divergence and cumulative flux at various depths due to all laser-generated electrons with energies in excess of 9 keV.

Time (ps)	Full div. angle (degrees)	Flux at 15 μm (Wcm^{-2})	Flux at 50 μm (Wcm^{-2})	Flux at 100 μm (Wcm^{-2})
0.75	32°	1.50×10^{20}	1.38×10^{20}	3.10×10^{19}
1.00	58°	1.92×10^{19}	2.29×10^{19}	2.98×10^{19}
1.50	69°	4.60×10^{18}	3.84×10^{18}	5.00×10^{18}
2.00	69°	2.56×10^{18}	1.63×10^{18}	1.10×10^{18}
4.00	69°	1.21×10^{17}	1.89×10^{17}	4.59×10^{16}

found that the energy in electrons above 1 MeV, transported within a 32° divergence angle, is 27%, 15%, and 7% of the laser energy at depths of 15 μm, 50 μm, and 100 μm, respectively. As a result of this initial narrow divergence, as much as 3.5 J of energy is transported to a depth of 100 μm by electrons with energies above 1 MeV.

IV. CONCLUSION

In conclusion, we have carried out experiments to study laser-generated electron beam divergence and energy transport at $I\lambda^2$ of $10^{20}\,\mathrm{Wcm}^{-2}\mu\mathrm{m}^2$. We used targets with a Cu tracer and a large carbon layer to reduce or eliminate electron refluxing from the rear and side surfaces of the target. Our data indicates that the time integrated electron beam divergence is wide [$(60 \pm 5)°$], consistent with the most recent published results. However, by using our experimental data to benchmark our modeling, we showed that the actual initial beam divergence is narrower. We have asserted that it is meaningless to attach a single divergence value to the electron beam in laser plasma interactions due time-dependence. A substantial fraction of energy is transported up to 100 μm with a divergence of 32°. Our current results hold for low prepulse levels. Our simulations show that, at a constant laser intensity, an increase of prepulse level results in an increase in beam divergence angle. As the amount of prepulse becomes larger, the laser propagation to the critical surface becomes increasingly complex due to instabilities such as filamentation. This will be highly dependent on the laser intensity, pulse duration, and f number. More work is needed to characterize the time evolution of the electron divergence and energy transport as a function of these quantities.

ACKNOWLEDGMENTS

K.A. acknowledges R. Stephens, E. Gaul, M. Donovan, M. Martinez, and Texas Petawatt Laser team for their support. This work was performed under the auspices of the US Department of Energy (DOE) under Contract No. DE-AC52-07NA27344, and DOE, National Nuclear Security Administration (NNSA) Grants No. DE-FC5208NA28512 and No. DEFG5209NA29547, awarded to the Center for High Energy Density Science at The University of Texas at Austin.

[1] K. U. Akli *et al.*, Phys. Rev. Lett. **100**, 165002 (2008).
[2] P. M. Nilson, W. Theobald, J. F. Myatt, C. Stoeckl, M. Storm, J. D. Zuegel, R. Betti, D. D. Meyerhofer, and T. C. Sangster, Phys. Rev. E **79**, 016406 (2009).
[3] G. Gregori *et al.*, Contrib. Plasma Phys. **45**, 284 (2005).
[4] R. A. Snavely *et al.*, Phys. Rev. Lett. **85**, 2945 (2000).
[5] A. Maksimchuk, S. Gu, K. Flippo, D. Umstadter, and V. Y. Bychenkov, Phys. Rev. Lett. **84**, 4108 (2000).
[6] S. Hatchett *et al.*, Phys. Plasmas **7**, 2076 (2000).
[7] C. Reich, I. Uschmann, F. Ewald, S. Düsterer, A. Lübcke, H. Schwoerer, R. Sauerbrey, E. Förster, and P. Gibbon, Phys. Rev. E **68**, 056408 (2003).
[8] H. Chen, S. C. Wilks, J. D. Bonlie, E. P. Liang, J. Myatt, D. F. Price, D. D. Meyerhofer, and P. Beiersdorfer, Phys. Rev. Lett. **102**, 105001 (2009).
[9] A. G. MacPhee *et al.*, Phys. Rev. Lett. **104**, 055002 (2010).
[10] M. Tabak, Phys. Plasmas **1**, 1626 (1994).
[11] R. B. Stephens *et al.*, Phys. Rev. E **69**, 066414 (2004).
[12] J. S. Green *et al.*, Phys. Rev. Lett. **100**, 015003 (2008).
[13] M. Storm *et al.*, Phys. Rev. Lett. **102**, 235004 (2009).
[14] K. L. Lancaster *et al.*, Phys. Rev. Lett. **98**, 125002 (2007).
[15] A. J. Mackinnon, M. Borghesi, S. Hatchett, M. H. Key, P. K. Patel, H. Campbell, A. Schiavi, R. Snavely, S. C. Wilks, and O. Willi, Phys. Rev. Lett. **86**, 1769 (2001).
[16] V. M. Ovchinnikov, D. W. Schumacher, G. E. Kemp, A. G. Krygier, L. D. V. Woerkom, K. U. Akli, R. R. Freeman, R. B. Stephens, and A. Link, Phys. Plasmas **18**, 112702 (2011).
[17] K. U. Akli *et al.*, Phys. Plasmas **14**, 023102 (2007).
[18] D. R. Welch, D. V. Rose, R. E. Clark, T. C. Genoni, and T. P. Hughes, Comput. Phys. Commun. **164**, 183 (2004).
[19] M. V. Ammosov, N. B. Delone, and V. K. Krainov, Sov. Phys. JETP **64**, 1191 (1986).
[20] M. P. Desjarlais, Contrib. Plasma Phys. **41**, 267 (2001).
[21] J. Halbleib, R. Kensek, G. Valdez, S. Seltzer, and M. Berger, IEEE Trans. Nucl. Sci. **39**, 1025 (1992).
[22] S. C. Wilks, W. L. Kruer, M. Tabak, and A. B. Langdon, Phys. Rev. Lett. **69**, 1383 (1992).
[23] K. Yasuike, M. H. Key, S. P. Hatchett, R. A. Snavely, and K. B. Wharton, Rev. Sci. Instrum. **72**, 1236 (2001).